PAPER

One-pot method for preparation of capsaicin-containing double-network hydrogels for marine antifouling

Pei Li,[ab] Xin Su,[b] Dezhao Hao,[c] Ming Yang,[b] Taijiang Gui,[d] Weiwei Cong,[d] Wenqiang Jiang, [iD][a] Xiuli Ge [iD] *[a] and Xinglin Guo [iD] *[b]

Marine biofouling which interferes with normal marine operation and also causes huge economic loss has become a worldwide problem. With the development of society, there is an urgent need to develop non-toxic and efficient anti-fouling strategies. Capsaicin is an environmentally friendly antifouling agent, but controlling the stable release of capsaicin from the coating is still a challenge to be solved. To achieve long-lasting antifouling property, in this work, we incorporate a derivative of capsaicin *N*-(4-hydroxy-3-methoxybenzyl)acrylamide (HMBA) to prepare double network (DN) hydrogels and make HMBA a part of the polymer network. Polyvinyl alcohol (PVA) has good hydrophilicity, and as a soft and ductile network, acrylamide (AM) and HMBA can polymerize to generate a rigid and brittle network. By adjusting the content of HMBA in the DN hydrogels, we can obtain a PVA–PAH*x* hydrogel with high mechanical strength, low swelling rate, and excellent antifouling effect, which provides a feasible way for the practical application of a hydrogel coating in long-term marine antifouling.

1. Introduction

Marine biofouling refers to the phenomenon in which some microorganisms, plants, and animals adhere to the surface of a material when it is submerged in the marine environment.[1–3] For ships, it can increase the friction on their bottom surface and their energy consumption.[4–6] It also accelerates material corrosion, increases maintenance costs,[7] and may increase the risk of biological invasion in regional seas.[6] A variety of strategies have evolved to address this world problem.[8–10]

For example, adding biocides to coatings to poison and kill organisms,[11] modifying surface micro-scale structures,[12] compounding low surface energy coatings,[13,14] constructing hydrophilic antifouling coatings such as PEG, amphoteric polymers, hydrogels and polysaccharide-based coatings, *etc.*,[15–20] are the common strategies to confront biofouling. Tributyltin-based compounds (TBT) incorporated into self-polishing coatings showed efficient antifouling properties and were applied after the 1960s.[21] However, TBT was found to induce deformations in fish and other species in the ocean, and as a result, coatings

containing organotin were removed from the market in 2003 and banned in 2008.[22] Some countries have banned the addition of heavy metal salts such as copper, zinc and lead to antifouling paints.[23] Observing the potential hazards of organic biocides and heavy metals to the marine environment, there is a growing focus on green antifouling strategies such as natural and environmentally friendly antifouling agents.[24,25]

Capsaicin has been reported in the literature to have excellent antifouling properties and has been developed for applications due to the low-risk assessment of the environment.[25–27] However, the difficulty of controlling the release rate of capsaicin when added to antifouling coatings has become a major problem and challenge.[28–30] Therefore, some studies have reported that analogs with more utility than capsaicin itself have become their substitutes.[31,32] As a capsaicin analog, HMBA is a monomer, which is similar to capsaicin in chemical structure, but it can polymerized with other monomers to synthesize antifouling materials, mostly for some membrane materials modification,[33–36] and antifouling copolymer coatings.[37–39] However, capsaicin analogs are mostly constructed as hydrophobic coatings due to a hydrophobic monomer, and hydrophobic surfaces in the ocean may have a significant affinity for organic pollutants thus causing biofouling.[3,40] Hydrophilic materials tend to be more attractive than hydrophobic materials in antifouling strategies.[41,42]

Hydrogel material is a three-dimensional hydrophilic polymers network containing a certain amount of water.[43] Hydrogel material contains many hydrophilic groups, which will cause the surface of the material to capture water molecules to form

[a]College of Environmental Science and Engineering, Qilu University of Technology (Shandong Academy of Sciences), Jinan, 250353, China. E-mail: gexiuli@qlu.edu.cn

[b]Key Laboratory of Science and Technology on High-Tech Polymer Materials, Institute of Chemistry, Chinese Academy of Sciences, Beijing 100190, China. E-mail: xlguo@iccas.ac.cn

[c]Laboratory of Bio-Inspired Smart Interface Science, Technical Institute of Physics and Chemistry, Chinese Academy of Sciences, Beijing 100191, China

[d]State Key Laboratory of Marine Coatings, Marine Chemical Research Institute Co. Ltd, China

a dense hydrated film, thereby achieving antifouling effects. To achieve a green antifouling strategy, in our previous work, the DN hydrogel with underwater superoleophobicity was prepared by the one-pot method.[44] Afterwards, hydrogels containing 3-(trimethoxysilyl)propylmethacrylate (TMSPMA) were prepared, and TMSPMA could be hydrolyzed on the surface of the gel into proto-silicate analogs to deceive algae to achieve specific anti-algae effects.[45] Hydrophilic/hydrophobic heterogeneous anti-biofouling hydrogels with well-regulated rehydration were also prepared.[46] All these works provide good ideas for hydrogel in the field of marine antifouling.

However, the mechanical properties of the hydrogel material itself are characterized by high water content and poor mechanical properties.[47] Gong prepared a DN hydrogel similar to cartilage in 2003, which inspired people to develop in the direction of tough performance.[48,49] Moreover, the construction of DN hydrogel has also broadened the multifunctional development of hydrogel materials, which can meet the needs of specific functions by changing the components of different networks.[50]

Inspired by the DN hydrogel to enhance its toughness[51] and hydrophilic–hydrophobic microzone help for antifouling.[52] In this work, PVA was selected as the first network, HMBA and AM generate polymer chains as a second network through polymerization reaction, DN hydrogel was constructed by one-pot method (Fig. 1). The hydroxyl groups on the PVA polymer chains form intermolecular hydrogen bonds with the phenolic hydroxyl groups, amino groups, and carbonyl groups on the PAH chains, which can help immobilize HMBA in the gel. The formation of hydrogen bonds between polymer chains can also increase the degree of cross-linking of the gel, which further changes the properties of the hydrogel. We finally obtained a hydrogel with low swelling, high toughness, and an excellent antifouling effect. It is proved that adding polymerizable capsaicin to the hydrogel coating can be better for practical needs, so it is an ideal strategy for marine antifouling applications.

2. Materials and methods

2.1 Experimental materials

N-Methylol acrylamide (N-MAM, 98%), guaiacol (Gal, 98%), magnesium sulfate (MgSO$_4$, 99.99%) were purchased from Aladdin. Acrylamide (AM, 99%) was obtained from Maclean. Concentrated sulfuric acid (H$_2$SO$_4$, AR) was purchased from Beijing Chemical Works. Polyvinyl alcohol (PVA, degree of hydrolysis 99%, 2800 degree of polymerization) was purchased from Sinopec Sichuan Vinylon Works. Dimethyl sulfoxide (DMSO) and ethanol absolute were received from Tianjin Concord Technology. N,N'-methylenebisacrylamide (MBAA) was received from Sigma-Aldrich, 2,2-dimethylacetophenone (DEAP, 98%) was purchased from J&K Chemical. The water used in the experiment was deionized water (DW). All reagents were used as received.

The subjects of this work to study the resistance to marine biofouling are mainly single-celled organisms diatoms,
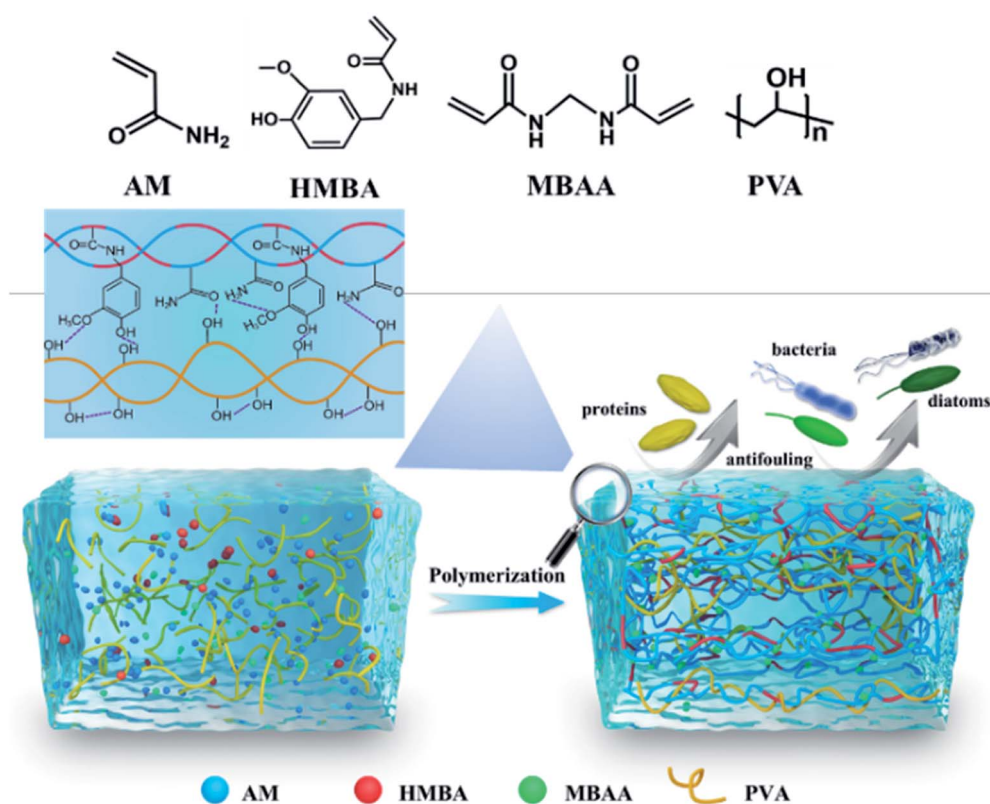

Fig. 1 A schematic illustration of the preparation and features of the PVA−PAH*X* gel.

including *Nitzschia closterium* and *Navicula*. *Nitzschia closterium* is a genus of warm, brackish, and semi-saltwater algae in the family *Nitzschiaceae*. *Navicula* sp. is a typical benthic attached diatom, belonging to the *Navicula*. The two algae were purchased from Xiamen Pulan Biotechnology Co., Ltd.

2.2   Experimental methods

2.2.1.   Synthesis of HMBA by Friedel–Craft. The capsaicin analogs *N*-(4-hydroxy-3-methoxy-benzyl)acrylamide (HMBA) is obtained by Friedel–Craft reaction.[31,35,37,38] First, add 200 mL of ethanol absolute as a solvent to a 500 mL round bottom flask, slowly add 20 mL of H_2SO_4, and stir evenly. Then add 80 g of *N*-MAM, 9.6 g of $MgSO_4$, and 100 g of Gal into the flask, and stir evenly with a magneton and continuously stirred for 7 days in a water bath at 35 °C. After the reaction was over, a large amount of white precipitate and the reddish-brown liquid was observed in the flask. The white precipitated material was filtered out through a vacuum water pump and a funnel, and the precipitated material was washed with a large amount of DW. At the same time, measure the pH of the washing liquid with a pH test paper, and wait until the washing liquid reaches neutrality. The washed white crude product was weighed and then recrystallized with absolute ethanol to obtain a relatively fine needle-like substance. By weighing, 81.2 g of the crude product was obtained, with a yield of 45.1%. After recrystallization, 62 g of fine product can be obtained, with a yield of 34.4%.

2.2.2.   Preparation of PVA SN hydrogel. Using DMSO and DW (80 wt% : 20 wt% mixture) as the solvent, 10 g of PVA particles were placed in a container containing 90 g of solvent and soaked for about 12 h so that the PVA particles were fully swollen in the solvent. The mixture was placed in a water bath and stirred continuously by a mechanical stirrer while heating slowly to maintain the water bath temperature at 100 °C for 2 h to ensure complete dissolution of PVA particles in the solvent, and we labeled the solution as "A". Subsequently, elimination of air bubbles in the solution. The hot PVA solution is poured into the mold. After it cools to room temperature, it is placed in a refrigerator and kept at −25 °C for 12 h, then removed to room temperature for 4 h, and the solvent was washed away to obtain PVA SN hydrogel.

2.2.3.   Preparation of PAH SN hydrogel. The preparation process of PAH SN hydrogel was carried out by a free radical polymerization reaction, in which the solvent was the same as that of PVA SN hydrogels. 28.432 g of AM was dissolved in solvent with 2.4 g of HMBA, 0.99 g MBAA and 1.33 g DEAP was added, and the total mass of the prepared solution is 100 g. The components in the solution were well dispersed by thorough stirring with a magnetic stirrer, and we labeled the solution as "B". Pour into the prepared mold and initiate free radical polymerization by UV (wavelength ≈ 365 nm) radiation in a dark box for 10 min to obtain a SN hydrogel of AM copolymerized with HMBA, which we named PAH.

2.2.4.   Preparation of PVA–PAHX DN hydrogels. The PVA–PAHX hydrogel was prepared by the "one-pot method",[53,54] and the tem-perature of the "A" solution during the above preparation of the PVA gel is maintained at 75 °C. Refer to the specific preparation steps of the PAH hydrogel, prepare the "B" solution with three different content of HMBA (2.4 g, 4.8 g, and 7.2 g), and heat it in a water bath to keep the temperature at 75 °C. Pour "A" and "B" solutions together in a ratio of 75 wt%-: 25 wt%, stir slowly to make them evenly mixed, then pour into the mold, and initiate polymerization (≈365 nm) for 10 min by UV radiation to obtain the formed gel. Put the gel in the freezer freeze for 12 h at −25 °C, and thaw for 4 h to obtain DN gel. Since the mass ratio of HMBA in DN hydrogel is 0.6%, 1.2%, and 1.8%, we named DN gel as PVA–PAHX (X is 0.6, 1.2, and 1.8).

2.2.5.   Preparation of PVA–PAM DN hydrogel. Referring to the preparation procedure of PVA–PAHX, the HMBA is not added in the configuration of "B". The other steps are exactly the same, and the prepared gel is named PVA–PAM. To reduce the influence of initiators, crosslinkers, and unreacted monomers on FITR, mechanical properties, surface wettability, and antifouling experiments during the preparation process, we rinsed and washed the prepared gel with deionized water. Soak for 96 h, change the water every 6 h.

2.3   Analysis and characterization

2.3.1.   FTIR and ¹H NMR analysis. The ^1H NMR spectra of HMBA was recorded with a Bruker NMR spectrometer Avance 400 III and dissolved with DMSO-*d* solvent. The chemical composition of the various hydrogels and HMBA were characterized by ATR-FTIR TENSOR-27 by vacuum drying the hydrogel components to remove water and then grinding them into powder, and the samples were mixed with potassium bromide powder pressed for testing in the scan range of 4000–400 cm^{-1} with 32 scans.

2.3.2.   Hydrogels swelling test. The gels swelling was performed by cutting the freshly prepared gels into the cylinder (diameter is 1 cm, height is 0.5 cm), respectively, and putting the different samples into 600 mL of water, keeping the temperature always at 25 °C. The data were recorded by taking out the samples and weighing them every 3 h during the first day, to better observe the changes of the hydrogels. Then, the hydrogels weight data were recorded at 12 h intervals until the dissolution equilibrium was reached. All the experiment samples are three parallel samples. The swelling ratio was calculated for each gel sample according to the formula.

$$\text{Swelling ratio (\%)} = (M_t - M_0)/M_0 \times 100\%$$

where M_0 is the initial weight of the gel and M_t is the weight of the gel at the specified time.

2.3.3.   Mechanical test. The compression experiment of hydrogel was carried out on a universal press (CTM2100 machine, Shanghai, China), and the hydrogel was cut into a cylinder with a diameter of 20 mm and a height of 15 mm, and the stress–strain curve of the gels was measured at a compression rate of 10 mm min^{-1} at 25 °C. The test was repeated three times for one kind of the gels, and the average value and standard error were obtained. Where the equation of compressive stress is

$$\sigma = F/A$$

where F is the force applied to the gels, and A is the cross-sectional area of the gels.

The calculation formula of compressive strain is:

$$\varepsilon = L/L_0$$

where L is the compression distance of the gel, and L_0 is the initial height of the gel.

The storage modulus of the hydrogels was measured with a rheometer (MCR 302, Anton Paar), and the hydrogels were cut into a cylindrical body with a diameter of 10 mm and a height of 2 mm. Shear frequency of 0.2% in the range of $\omega = 0.1\text{--}100$ rad s^{-1} with a strain amplitude of $\gamma_0 = 0.2\%$ at 23 °C to carry out.

2.3.4. Structural characterization. The gels were soaked in 600 mL of ionized water for 96 h, changing the water every 6 h. After reaching the swelling equilibrium, the excess water was wiped off the surface, cut into thin slices of the specified size, placed in a container, and cooled by pouring liquid nitrogen. The treated hydrogels were freeze-dried in a freeze-dryer 24 h. The dried hydrogels were sprayed with platinum to observe the internal structure of hydrogels in a scanning electron microscope (SEM).

2.3.5. Wettability test. The hydrogels in swelling equilibrium were cut into $2.5 \times 2.5 \times 0.1$ cm slices and the contact angles (CA) for water in air and oil under water were measured by a contact angle system (OCA-40 Micro, Germany) for the hydrogel samples, and all water used was DW, and 1,2-dichloroethane was used for the oil. The water in the tube was dropped onto the upper surface of the hydrogels in a dose of 2 μL through a micro sampler, and the measurement was performed at different positions for each sample, and five readings were taken and the magnitude of the contact angle was recorded, and the mean value and standard deviation were calculated. The procedure for the determination of underwater oil was to fix the hydrogel sample in a trans-parent sink so that it was in a horizontal position, and 2 μL of 1,2-dichloroethane in water was dropped on the surface of the hydrogel, and 5 positions were also selected for recording the readings and calculating the mean value and standard deviation.

2.3.6. Gel antifouling properties. The antifouling experiments of hydrogels were performed by analyzing adhering algae by autofluorescence images. Before starting the antifouling test, all samples were immersed in sterile seawater for three days to reach equilibrium. Typically, samples were placed in six-well plates and 10 mL of diatom suspension was then added to each well. After incubation in a constant temperature incubator at a constant temperature of 23 °C for 72 h, every day (12 h of light and 12 h of darkness, 7 am to 7 pm for light conditions and 7 pm to 7 am for dark conditions), the surface of the hydrogel samples was washed with sterile seawater to remove unattached diatoms. *Navicula* adhesion and *Nitzschia closterium* adhesion were two separate experiments, two samples of each gel were prepared with an area of approximately 2×2.5 cm, and a total of 20 measurement points were taken for each sample during the observation process, and the samples were evaluated. The samples were observed using a fluorescence detector (DP80). The number of attached algae was counted by image J software.

3. Results and discussion

3.1 Characterization of the chemical structures

In the present work, we analyzed the HMBA by ^{1}H-NMR and the identification results are shown in Fig. 2a, ^{1}H-NMR (DMSO, ppm): 8.85 (s, 1H, O–H), 8.45 (s, 1H, N–H), 6.70 (d, 2H, –CH=CH–aromatic), 6.23 (d, 2H, CH_2=), 5.58 (t, 1H, CH=), 4.23 (d, 2H, CH_2–NH), 3.73(s, O–CH_3).

Fig. 2b shows the IR spectrum of HMBA, PVA, PAH, and PVA–PAH0.6 hydrogels. It can be regarded as the strong absorption peak caused by phenolic hydroxyl (OH–) on the benzene ring in 3325 cm^{-1}, and the corresponding absorption bands at 1654 cm^{-1} can be assigned to stretching of carbonyl (C=O) in the acid amide of HMBA monomer. It also shows that two absorption peaks at 1597 cm^{-1} and 1523 cm^{-1}, which are the vibrations of the (C=C) skeleton on the aromatic ring. From the above, it can be concluded that the HMBA monomer has been successfully synthesized.

For PVA gel, the strong band at 3857–2985 cm^{-1} corresponds to the strong (–OH) band typical of intermolecular and intra-molecular hydrogen bonding. The FTIR spectrum of PAH shows peaks appears near 1654 cm^{-1} corresponding to the secondary amide stretching vibration, the stretching vibration peak of the secondary amide-association state appears near 3421 cm^{-1}, the benzene ring skeleton vibration peak appears near 1652 cm^{-1}, 1487 cm^{-1}, and 1456 cm^{-1}, and the carbon–oxygen vibration peak of the phenyl hydroxyl group appears near 1247 cm^{-1}. These all indicate the existence of HMBA structural units in the polymer molecules. The associative stretch vibration peaks of primary amides appear at 3200–3350 cm^{-1}, indicating the existence of AM structural units in the polymer molecules. Similarly, for PVA–PAH0.6, peaks at 1652 cm^{-1}, 1487 cm^{-1}, and 1456 cm^{-1} can be detected with the benzene ring skeleton vibration, thus it can be judged that the gel PAH and PVA–PAH0.6 have been polymerized and formed.

3.2 Swelling properties of hydrogels

Generally speaking, the degree of swelling of the hydrogels as coatings has a critical impact in practical applications. The swelling behavior of hydrogels is influenced by multiple factors, such as the crosslink density of the material itself, hydration, ion concentration in the aqueous environment, pH, *etc.* Fig. 3a shows the swelling behavior of different gels in deionized water with time. It can be seen that the hydrogels showed a large weight change in the first 3 h after being placed in water, except for the PVA gels which showed a sharp increase in swelling behavior, and PVA showed a special behavior of −1.52%. Immediately afterward, the swelling rate of each component gels showed a slow increase, and the swelling rate of PVA continued to show steady negative growth. Within 24 h, all hydrogels reached the peak of their swelling rate variation, and then the gels variation showed a slow decrease until equilibrium was reached. Among all the hydrogels, the swelling rate of
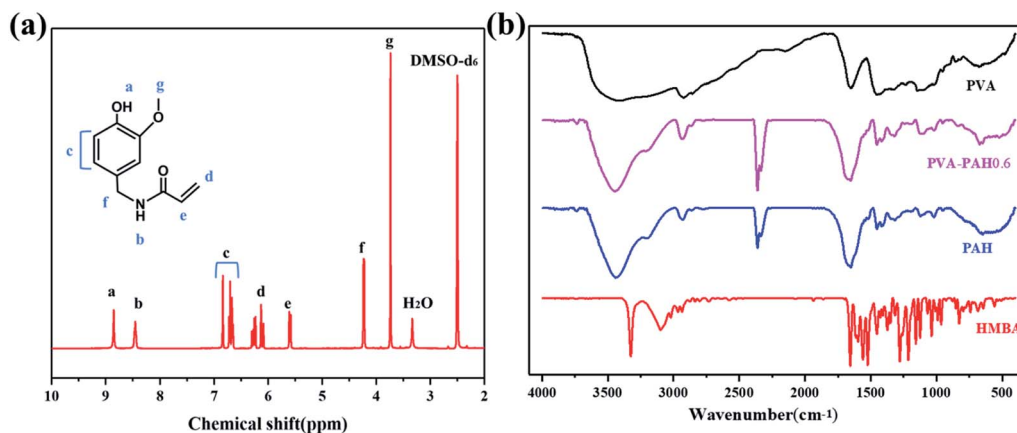
Fig. 2 (a) The ¹H NMR spectrum of HMBA, (b) the FT-IR spectrum of HMBA, PVA, PAH and PVA−PAH0.6.

PAH is the largest for the reason that PAH has the largest pores in SEM (Fig. 6), in addition, PAH is rich in hydroxyl and amino to have a better affinity with water molecules. PVA–PAM also shows a faster rate of water absorption, probably because of PVA and AM composite, where the hydrophilic group can quickly absorb water, but the formation of intermolecular hydrogen bonds instead of inhibiting their own swelling. It can be seen by PVA–PAH0.6 and PVA–PAM that HMBA slows down the water absorption rate of the gel in DN, and the water absorption rate of the gel is slower as the amount of HMBA added increases. These are attributed to the fact that HMBA is a hydrophobic monomer.

From Fig. 3b, it can be seen that only PVA is collapsed in water, and the reason is that PVA forms a good homogeneous network because the mixture of DMSO and water is a good solvent, and when placed in deionized water, the hydrogen bonds bound to DMSO in PVA are reduced, from which a more dense hydrogen bond is formed in the gel, and thus the swelling rate of PVA shows negative growth. The appearance of the PAH shows a large increase. Since PAM itself has a strong water

absorption capacity, it can be seen from SEM (Fig. 6) that the pores of the gel are also the largest. On the other hand, the equilibrium swelling rate of DN gels decreased gradually with the increase of HMBA, because HMBA is a hydrophobic monomer. Equally important, with reference to the SEM images (Fig. 6) of hydrogels, the swelling behavior of hydrogels is also related to the cross-link density. As the cross-link density increases, the cross-link points in the cross-link network increase, the chain segments between the cross-link points become shorter, and the micropores in the network structure become smaller, so the swelling ratio decreases.

3.3 Mechanical properties of hydrogels

When hydrogels coatings are needed to meet practical needs in marine antifouling work, good mechanical properties are usually required to combat the complex marine environment, where the measured parameters are generally compressive strength and energy storage modulus. A universal testing machine was used to test the hydrogels after swelling equilibrium in water to examine the SN hydrogels and DN hydrogels
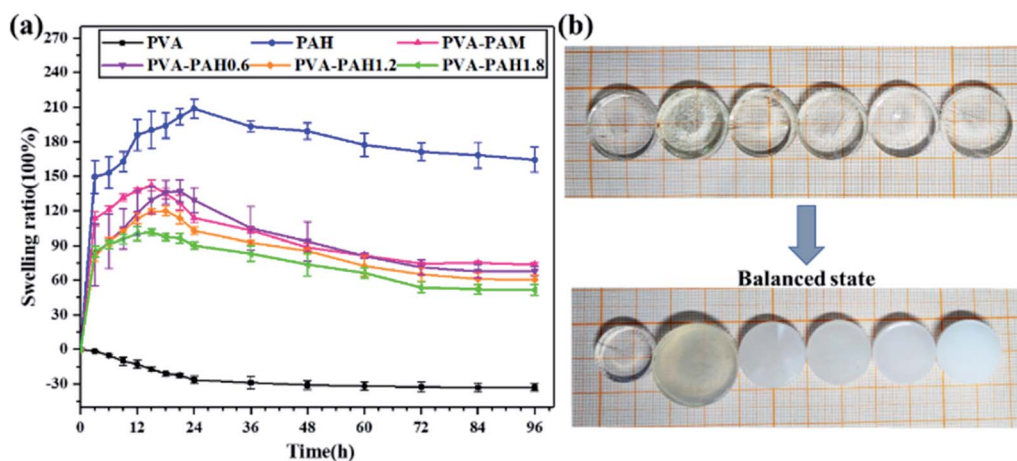

Fig. 3 (a) The swelling rate of the hydrogel changes with time. (b) Comparison of various gels (from left to right are PVA, PAH, PVA−PAM, PVA−PAH0.6, PVA−PAH1.2, PVA−PAH1.8) before and after swelling balance.

performance tests, and also to examine the effect of HMBA addition on the mechanical properties of DN hydrogels. The measures we took were to subject the prepared SN gels PVA, PAH, and DN gels PVA–PAH*X* to uniaxial compression tests with increasing HMBA concentration and to test the hydrogels after swelling equilibrium under the condition of 80% compressive strain.

From Fig. 4a, it can be seen that the compressive stress of DN hydrogel is higher than those of the SN hydrogels, and the recorded data show that the stress of the SN hydrogel PAH is the smallest in the compression process of the hydrogels, and the stress of the PVA are higher than those of PAH only. The parameters of DN hydrogels are significantly higher than those of SN hydrogels. With the increase of HMBA addition, the stress of DN hydrogels with high HMBA content is higher than that of low HMBA content. In the comparison of DN hydrogels, it can be seen that with the increase of HMBA content, the compressive stress (σ) of DN hydrogel at 80% strain gradually increases from 2.05 MPa to 3.21 MPa, and the mechanical properties are significantly higher than that of SN hydrogels PAH and PVA. The compressive stress (σ) of DN hydrogels gradually increased from 2.05 MPa to 3.21 MPa. In contrast, the storage modulus of the DN gels was much higher than any SN gels (Fig. 4b). Besides, the order size of the hydrogels G' is PVA–PAH1.8 > PVA–PAH1.2 > PVA–PAH0.6 > PVA–PAM > PVA > PAH, which indicated that DN hydrogels are highly elastic. The introduction of DN in the hydrogel can well improve the strength and toughness of the hydrogel, in which the proportion of HMBA in the PAH gel can be adjusted to achieve this purpose.

Generally, the hydrogels are affected by the cross-linking of molecular chains during its construction. In the construction of PVA–PAH*X* hydrogels, the PVA network is physically cross-linked by hydrogen bonding. While the content of MBAA in the PAH network is constant, the change of HMBA content plays a decisive role in improving the mechanical strength of the gels, and with the increase of HMBA content, the mesh of PVA–PAH*X* becomes denser and the mechanical strength of the hydrogel gradually increases.

Fig. 5a clearly shows that the SN gel PAH can be easily broken under extrusion conditions, PVA gel is a soft network although it will not break it is difficult to return to the original shape after a single extrusion, while the DN gel PVA–PAH0.6 still maintains its initial shape after extrusion, has good elasticity and toughness, and has excellent mechanical properties compared with any SN gels. For convenience, Fig. 5b shows the cutting of PVA–PAH0.6 alone was demonstrated and the gel remained intact under the forceful cutting of the steel ruler.

3.4 Surface microstructure properties of hydrogels

A hydrogel is a three-dimensional network-like structure, inside which is usually filled with a large amount of water. Hydrogels material are usually porous structures, which satisfy in the ocean will exchange a large amount of water flux with the external environment, where the size of the pores in the network affects the rate of water exchange between the hydrogels and the external environment and its properties. The surface structures of hydrogels observed by swept surface electron microscopy are shown in the figure below.

It can be seen that the PVA gel shows a small pore arrangement with a pore diameter of 0.2–3 μm, from which it can be seen that although the pores of the PVA are more numerous, the distribution of the pore walls between the voids is thicker, probably because the solvent in the PVA is a mixture of DMSO and water in the process of freezing does not appear enough ice crystals inside the gel. It is easy to see that the pores of PAH are the largest, and their pore diameters are distributed in the range of 10–40 μm, while the pores of PVA–PAM are between those of PVA and PAH0.6, and the voids are about 1–8 μm, and the pores are more densely arranged with thinner pore walls. When HMBA was added, we can see that the pores of PAH0.6 did not change much compared with PVA–PAM, but the pore walls became thicker, which was due to the increase of HMBA. With the increase of HMBA content, the pores of PVA–PAH1.2 and PVA–PAH1.8 are obviously smaller, and the pore diameter is distributed in 0.3–4 μm, while the pore distribution of PVA–PAH1.8 with the most HMBA content is smaller and more
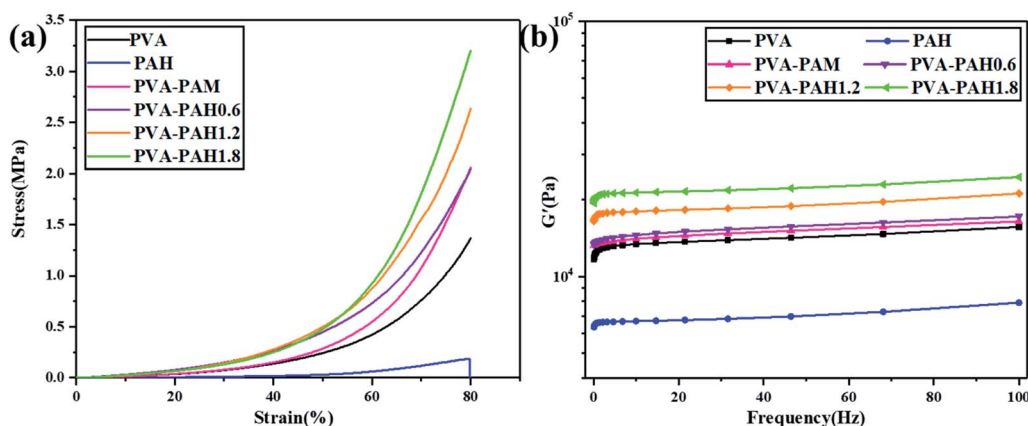

Fig. 4 The effects of SN and DN with the addition of HMBA after equilibrium swelling on (a) uniaxial compression performance and (b) storage modulus in rheology are studied.
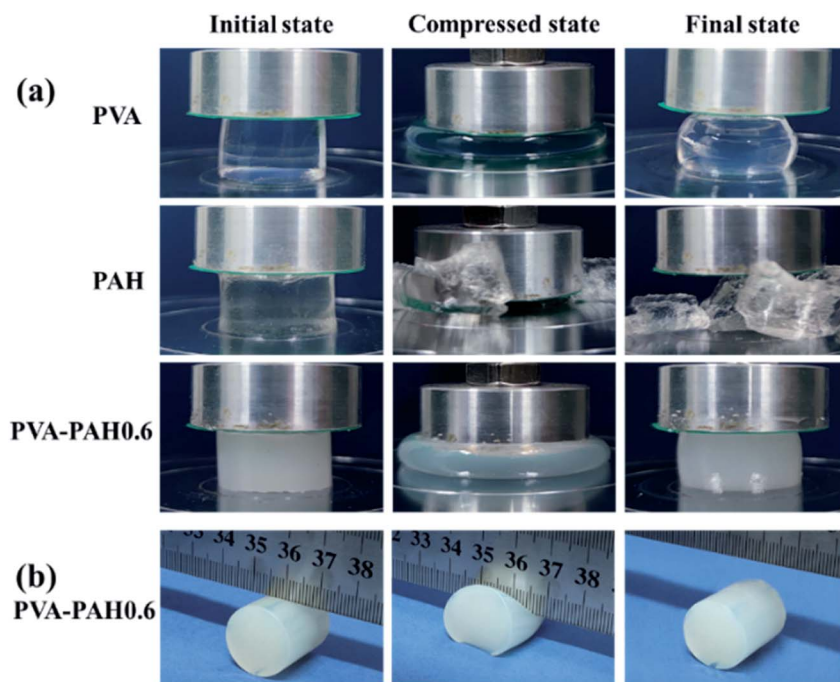
Fig. 5 (a) The hydrogel compression process, compressed at a rate of 10 mm min^{-1} to a strain of 80%. (b) Cut to the lowest point in the middle of the PVA–PAH0.6 by means of a steel ruler.

uniform than PVA–PAH1.2, and the pore wall is also thicker. The pore size of PVA, PAH, and PVA–PAHX is positively correlated with the water content of the gels.

The degree of cross-linking of hydrogels can also be seen in the figure. Comparing the DN gels, it can be seen that with a constant MBAA content, the increase of HMBA content can increase the intermolecular hydrogen bonding arrangement of polymer chains thus increasing the cross-linking density of the gels and increasing the cross-linking point, which makes the pores of DN gels smaller and makes the pore walls thicker, thus better explaining the swelling behavior and mechanical properties of the hydrogels.

3.5 The wettability of hydrogel

The wettability of the hydrogel surface is also an important part of the antifouling performance test, and hydrogels have an important development prospect as a hydrophilic material to prevent biological adhesion in the ocean. For this reason, we tested the static contact angle of water droplets in the air and the static contact angle of oil droplets in water for each component gels, where 2 μL of deionized water was used for water droplets and 2 μL of 1,2-dichloroethane for oil droplets. As shown in Fig. 7a, the CA of PVA and PVA–PAM were 11.2° ± 1.5° and 11.4 ± 3.8°, respectively, with the smallest CA indicating good hydrophilicity. The CA of PAH was 23.2 ± 3.7°
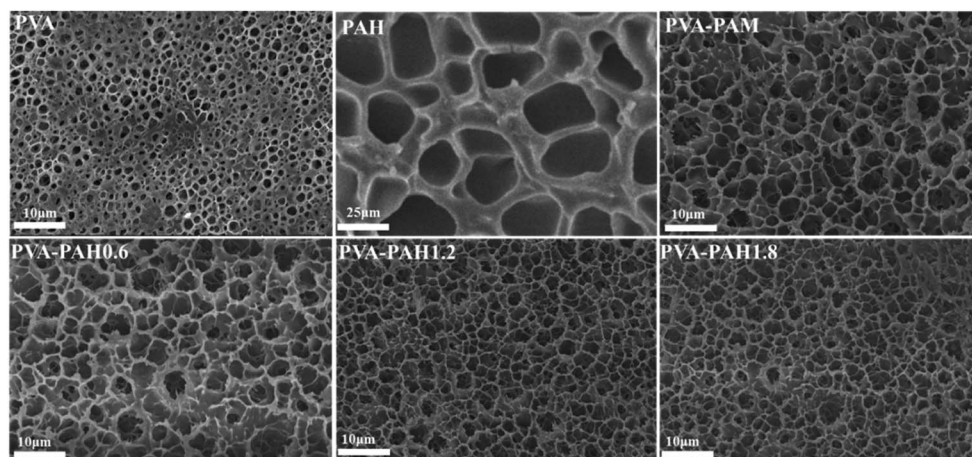

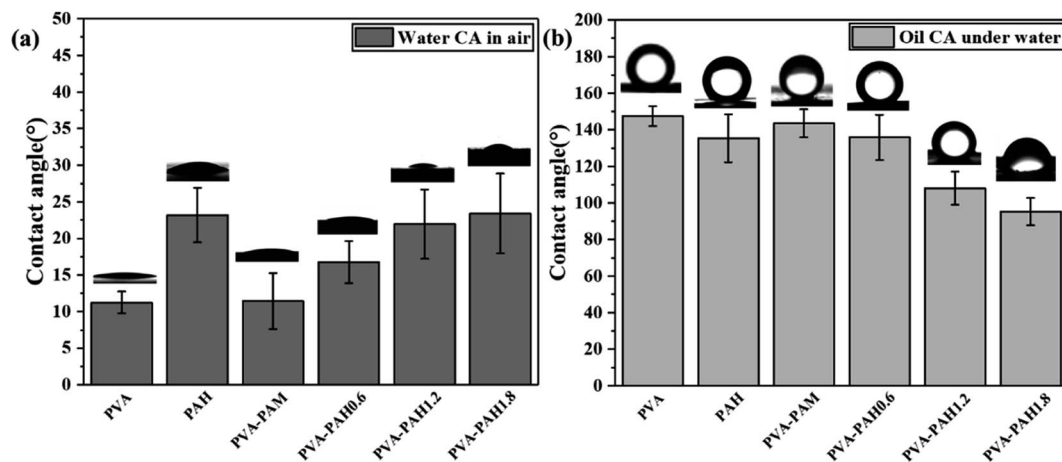**Fig. 6** SEM images of the pore size comparison of SN gels and DN gels with different HMBA contents.

Fig. 7 Static contact angle of hydrogel (a) CA of water in the air (b) CA of underwater oil.

which also indicated that the PAH gel with capsaicin addition also showed hydrophilicity. With the increase of HMBA content in the gels, the PVA–PAHX also showed an increasing trend of CA size although they were hydrophilic. Overall, HMBA, a hydrophobic monomer, weakens the hydrophilic properties of the gels, but the gels still exhibit hydrophilic properties.

From Fig. 7b, it is easy to see that the CA of PVA and PVA–PAM are $147.5° \pm 5.6°$ and $143.5° \pm 7.7°$, respectively, showing strong oleophobic, while the CA of PAH is $135.4° \pm 13.1°$ with some hydrophobic molecules (HMBA). We can attribute this to the fact that the gel has many hydrophilic groups which absorbs a large amount of water, giving the body a good oleophobic property. It can also be seen that with the increase of HMBA

addition in the PVA–PAHX, the CA also decreases and shows slight oleophilicity. We can explain that the HMBA monomer is uniformly distributed on the surface of the gels after reaching the swelling equilibrium in the gels system, and its components make the surface of the gels have slightly oleophilic.

Surprisingly, the PVA network has excellent hydrophilicity, while the PAH network is obtained by copolymerization of hydrophilic AM monomer and hydrophobic HMBA monomer, which has hydrophilic. In the DN gels network, PVA–PAM without HMBA has hydrophilic and superoleophilic properties, and with the increase of HMBA content also has an oleophilic ability. It indicates that HMBA is distributed on the surface of PVA–PAHX, which can explain to some extent that capsaicin on
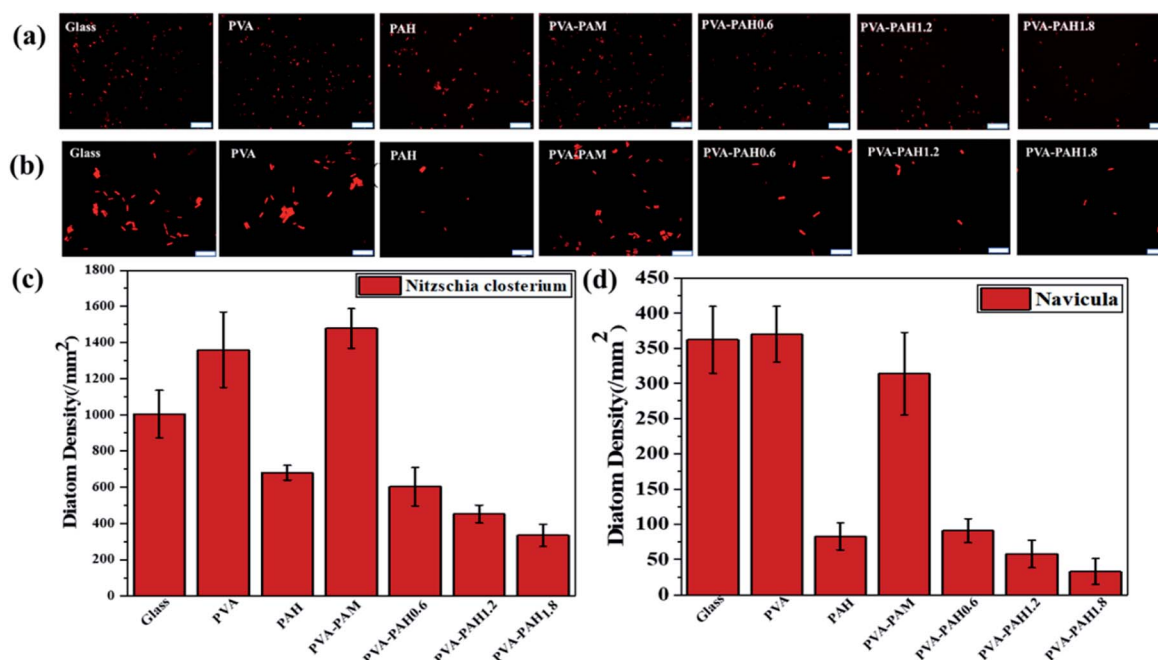

Fig. 8 Anti-diatom adhesion performance (a) and (b) fluorescence micrographs pictures of the densities of adhered *Navicula* sp. and *Navicula* (the ruler in the picture is 50 μm). (c) and (d) Statistical chart showing diatom adhesion ($p < 0.01$).

the surface of DN gels is convenient to contact with marine adherent organisms to play an antifouling effect.

3.6 The antifouling properties of hydrogel

To further explore the antifouling performance of hydrogels, we tested the adhesion ability of various gels to *Nitzschia closterium* and *Navicula* sp. respectively under fully simulated marine environment (reference experimental method). Biofouling counts are shown in Fig. 8a and b, and in general to increase the control we selected glass slice samples to increase the indication of the good activity of algae. Firstly, it can be observed that after three days of incubation period all substrates had biologically active algae attached on top.

As shown in Fig. 8c, the glass as control is about 1004 diatoms per mm^2, and the hydrogel PVA and PVA–PAM without HMBA are about 1360 diatoms per mm^2 and 1478 diatoms per mm^2, respectively, with a large number of diatoms adhering to its surface, indicating poor antifouling properties. The number of diatoms was suppressed to some extent for the fraction with HMBA added, for example, 680 diatoms per mm^2 for PAH0.6, while for DN gel with different loading of HMBA, the number of diatoms showed a decrease with the increase of HMBA content.

From Fig. 8b and d, the micrographs and diatom counts were observed. The highest amount of adherence was PVA–PAM and reached 368 diatoms per mm^2 which indicates that the DN gel without HMBA added adhered more diatoms, while AH had some inhibitory effect compared to the other components without HMBA added. Comparing the number of diatoms attached to PAH and PVA–PAHX, the HMBA content in PVA–PAHX is not as high as that of PAH, but it is better than the former in terms of anti-fouling and anti-algae effects. And the adhesion of the PVA network combined with the PAH network was reduced, which indicates that the composition of the double network helps HMBA to play a better antifouling ability. And with the increase of HMBA content, the antifouling effect was also significantly improved.

4. Conclusions

In summary, we have prepared DN hydrogels coating containing capsaicin analogs by the one-pot method based on the green strategy. The double network structure can ensure the high strength mechanical properties of the hydrogels and can lock HMBA well in the materials. Simultaneously, the PVA–PAHX has the properties of low swelling ratio, high hydrophilicity, and superoleophobicity. More importantly, the introduction of HMBA into the hydrogels coating has shown excellent antifouling effect. It is worth noting that the HMBA immobilized on the DN hydrogels can achieve a long-lasting antifouling effect rather than the release model. This work will contribute to the practical application of hydrogel materials in the field of marine antifouling.

Conflicts of interest

There are no conflicts to declare.

Acknowledgements

References

1 I. Amara, W. Miled, R. B. Slama and N. Ladhari, *Environ. Toxicol. Pharmacol.*, 2018, **57**, 115–130.

2 J. A. Batista-Andrade, S. S. Caldas, R. M. Batista, I. B. Castro, G. Fillmann and E. G. Primel, *Environ. Pollut.*, 2018, **234**, 243–252.

3 J. A. Callow and M. E. Callow, *Nat. Commun.*, 2011, **2**, 244.

4 R. B. Bodkhe, S. J. Stafslien, J. Daniels, N. Cilz, A. J. Muelhberg, S. E. M. Thompson, M. E. Callow, J. A. Callow and D. C. Webster, *Prog. Org. Coat.*, 2015, **78**, 369–380.

5 D. Carteau, K. Vallée-Réhel, I. Linossier, F. Quiniou, R. Davy, C. Compère, M. Delbury and F. Faÿ, *Prog. Org. Coat.*, 2014, **77**, 485–493.

6 D. M. Yebra, S. Kiil and K. Dam-Johansen, *Prog. Org. Coat.*, 2004, **50**, 75–104.

7 M. P. Schultz, *Biofouling*, 2007, **23**, 331–341.

8 S. Anthony Yesudass, S. Mohanty, S. K. Nayak and C. C. Rath, *Eur. Polym. J.*, 2017, **96**, 304–315.

9 K. A. Dafforn, J. A. Lewis and E. L. Johnston, *Mar. Pollut. Bull.*, 2011, **62**, 453–465.

10 A. Turner, *Mar. Pollut. Bull.*, 2010, **60**, 159–171.

11 S. M. Jung, J. S. Bae, S. G. Kang, J. S. Son, J. H. Jeon, H. J. Lee, J. Y. Jeon, M. Sidharthan, S. H. Ryu and H. W. Shin, *Mar. Pollut. Bull.*, 2017, **124**, 811–818.

12 S. Krishnan, C. J. Weinman and C. K. Ober, *J. Mater. Chem.*, 2008, **18**, 3405–3413.

13 W. Jiang, Q. Niu, L. Cheng, T. Zhou and H. Xie, *Corros. Rev.*, 2020, **38**, 331–338.

14 E. Lindner, *Biofouling*, 1992, **6**, 193–205.

15 J. Yang, B. Xue, Y. Zhou, M. Qin, W. Wang and Y. Cao, *Adv. Mater. Technol.*, 2021, **6**, 2000911.

16 F. Hong, L. Xie, C. He, J. Liu, G. Zhang and C. Wu, *J. Mater. Chem. B*, 2013, **1**, 2048–2055.

17 L. Xie, F. Hong, C. He, C. Ma, J. Liu, G. Zhang and C. Wu, *Polymer*, 2011, **52**, 3738–3744.

18 T. Murosaki, N. Ahmed and J. Ping Gong, *Sci. Technol. Adv. Mater.*, 2011, **12**, 064706.

19 P. Lundberg, A. Bruin, J. W. Klijnstra, A. M. Nystrom, M. Johansson, M. Malkoch and A. Hult, *ACS Appl. Mater. Interfaces*, 2010, **2**, 903–912.

20 T. Murosaki, T. Noguchi, K. Hashimoto, A. Kakugo, T. Kurokawa, J. Saito, Y. M. Chen, H. Furukawa and J. P. Gong, *Biofouling*, 2009, **25**, 657–666.

21 B. Antizar-Ladislao, *Environ. Int.*, 2008, **34**, 292–308.

22 J. T. Koning, U. E. Bollmann and K. Bester, *Mar. Pollut. Bull.*, 2020, **158**, 111402.

23 S. Satheesh, M. A. Ba-akdah and A. A. Al-Sofyani, *Electron. J. Biotechnol.*, 2016, **21**, 26–35.

24 M. S. Selim, M. A. Shenashen, S. A. El-Safty, S. A. Higazy, M. M. Selim, H. Isago and A. Elmarakbi, *Prog. Mater. Sci.*, 2017, **87**, 1–32.

25 K. V. Thomas and S. Brooks, *Biofouling*, 2010, **26**, 73–88.

26 J. Wang, T. Shi, X. Yang, W. Han and Y. Zhou, *Chemosphere*, 2014, **104**, 85–90.

27 M. B. Angarano, R. F. McMahon, D. L. Hawkins and J. A. Schetz, *Biofouling*, 2007, **23**, 295–305.

28 X. Hao, S. Chen, D. Qin, M. Zhang, W. Li, J. Fan, C. Wang, M. Dong, J. Zhang, F. Cheng and Z. Guo, *Mater. Sci. Eng., C*, 2020, **108**, 110361.

29 Z. Lu, Z. Chen, Y. Guo, Y. Ju, Y. Liu, R. Feng, C. Xiong, C. K. Ober and L. Dong, *ACS Appl. Mater. Interfaces*, 2018, **10**, 9718–9726.

30 W. Wang, X. Hao, S. Chen, Z. Yang, C. Wang, R. Yan, X. Zhang, H. Liu, Q. Shao and Z. Guo, *Polymer*, 2018, **158**, 223–230.

31 X. Wang, L. Yu, F. Li, G. Zhang, W. Zhou and X. Jiang, *J. Food Biochem.*, 2019, **43**, e13061.

32 X. Wang, L. Yu, Y. Liu and X. Jiang, *Sci. Total Environ.*, 2020, **710**, 136361.

33 X. L. Gao, H. Z. Wang, J. Wang, X. Huang and C. J. Gao, *J. Membr. Sci.*, 2013, **445**, 146–155.

34 Y. Tang, L. Zhang, C. Shan, L. Xu, L. Yu and H. Gao, *J. Membr. Sci.*, 2020, **610**, 118233.

35 J. Wang, H. J. Sun, X. L. Gao and C. J. Gao, *Appl. Surf. Sci.*, 2014, **317**, 210–219.

36 X. Zhan, G. Zhang, X. Chen, R. He, Q. Zhang and F. Chen, *Ind. Eng. Chem. Res.*, 2015, **54**, 11312–11318.

37 X. Chen, G. Zhang, Q. Zhang, X. Zhan and F. Chen, *Ind. Eng. Chem. Res.*, 2015, **54**, 3813–3820.

38 H. Wang, J. Jasensky, N. W. Ulrich, J. Cheng, H. Huang, Z. Chen and C. He, *Langmuir*, 2017, **33**, 13689–13698.

39 X. Wang, X. Jiang and L. Yu, *Prog. Org. Coat.*, 2021, **160**, 106515.

40 L. Schardt, A. Martinez Guajardo, J. Koc, J. L. Clarke, J. A. Finlay, A. S. Clare, H. Gardner, G. W. Swain, K. Hunsucker, A. Laschewsky and A. Rosenhahn, *Macromol. Rapid Commun.*, 2021, e2100589, DOI: **10.1002/marc.202100589**.

41 X. Lin, X. Huang, C. Zeng, W. Wang, C. Ding, J. Xu, Q. He and B. Guo, *J. Colloid Interface Sci.*, 2019, **535**, 491–498.

42 R. Wanka, F. Koschitzki, V. Puzovic, T. Pahl, E. Manderfeld, K. Z. Hunsucker, G. W. Swain and A. Rosenhahn, *ACS Appl. Mater. Interfaces*, 2021, **13**, 6659–6669.

43 W. Zhang, X. Liu, J. Wang, J. Tang, J. Hu, T. Lu and Z. Suo, *Eng. Fract. Mech.*, 2018, **187**, 74–93.

44 H. Li, D. Hao, J. Fan, S. Song, X. Guo, W. Song, M. Liu and L. Jiang, *J. Mater. Chem. B*, 2016, **4**, 4662–4666.

45 W. Chen, D. Hao, X. Guo, W. Hao and L. Jiang, *J. Mater. Chem. A*, 2018, **6**, 19125–19132.

46 X. Su, D. Hao, X. Xu, X. Guo, Z. Li and L. Jiang, *ACS Appl. Mater. Interfaces*, 2020, **12**, 25316–25323.

47 R. Bai, B. Chen, J. Yang and Z. Suo, *J. Mech. Phys. Solids*, 2019, **125**, 749–761.

48 T. Nonoyama and J. P. Gong, *Proc. Inst. Mech. Eng., Part H*, 2015, **229**, 853–863.

49 J. P. Gong, Y. Katsuyama, T. Kurokawa and Y. Osada, *Adv. Mater.*, 2003, **15**, 1155–1158.

50 R. Bai, J. Yang and Z. Suo, *Eur. J. Mech. A/Solids*, 2019, **74**, 337–370.

51 S. Ahmed, T. Nakajima, T. Kurokawa, M. Anamul Haque and J. P. Gong, *Polymer*, 2014, **55**, 914–923.

52 X. Su, M. Yang, D. Hao, X. Guo and L. Jiang, *J. Colloid Interface Sci.*, 2021, **598**, 104–112.

53 H. Liu, B. Lepoittevin, C. Roddier, V. Guerineau, L. Bech, J.-M. Herry, M.-N. Bellon-Fontaine and P. Roger, *Polymer*, 2011, **52**, 1908–1916.

54 Q. Chen, H. Chen, L. Zhu and J. Zheng, *J. Mater. Chem. B*, 2015, **3**, 3654–3676.